Automatika
Journal for Control, Measurement, Electronics, Computing and Communications

ISSN: (Print) (Online) Journal homepage: www.tandfonline.com/journals/taut20

The analysis of damage mechanisms and vibration effects caused by cut blasting under various void shapes

Huifeng Qin, Yan Zhao, Hailong Wang & Lijie Ge

To cite this article: Huifeng Qin, Yan Zhao, Hailong Wang & Lijie Ge (2024) The analysis of damage mechanisms and vibration effects caused by cut blasting under various void shapes, Automatika, 65:4, 1506-1516, DOI: 10.1080/00051144.2024.2399337

To link to this article: https://doi.org/10.1080/00051144.2024.2399337

Published online: 10 Sep 2024.

AUTOMATIKA
2024, VOL. 65, NO. 4, 1506–1516
https://doi.org/10.1080/00051144.2024.2399337

The analysis of damage mechanisms and vibration effects caused by cut blasting under various void shapes

Huifeng Qin[a], Yan Zhao[b,c,d,e], Hailong Wang[a,b] and Lijie Ge[b]

[a]Shijiazhuang tiedao University, Shijiazhuang Civil Engineering College, Hebei Province, People's Republic of China; [b]Hebei University of Architecture,Zhangjiakou Civil Engineering College, Hebei Province, People's Republic of China; [c]School of Mechanics and Civil Engineering, China University of Mining and Technology (Beijing), Beijing, People's Republic of China; [d]Key Laboratory of Civil Engineering Diagnosis, Reinforcement and Disaster Prevention, Zhangjiakou, People's Republic of China; [e]Zhangjiakou BIM Engineering Technology Innovation Center, Zhangjiakou, People's Republic of China

ABSTRACT

The effect of the void shape on cut blasting is investigated by establishing a damage analysis model for a void using an improved calculation formula for stress on the wall of the void. Additionally, an optimization scheme is provided for the "square void cutting theoretical model." The vibration effect of the rock mass outside the excavation area is simultaneously monitored, and its validity is substantiated through experimental and simulation-based verification. The findings indicate that the variation of q2sinθ over time aligns with the dynamic loading process of wall stress in holes. Under the influence of longitudinal waves, thin-walled circular damage occurs, and tensile effects from reflected waves are influenced by impedance. In a square void cutting model, two-stage stress waves cause tensile shear damage and inward collapse in the rock mass along hole walls. The explosive energy generated by square holes significantly contributes to fragmentation of rock masses. The circular empty-hole cutting model generates significant vibrations in central areas due to resistance. Vibration velocity in 45° direction for circular holes is lower than that for square voids outside cuts while vibration velocity remains equivalent between circular and square holes at 90° direction.

ARTICLE HISTORY
Received 17 February 2024
Accepted 27 August 2024

KEYWORDS
Damage mechanism; longitudinal wave impact testing; dynamic evolution of stress; numerical simulation of rocks; vibration influence

1. Introduction

The interaction between gas explosions and the superposition of stress waves during cut blasting operations is a highly intricate phenomenon, and accurately analyzing the failure mechanism of surrounding rock is crucial for effectively controlling damage caused by cutting. However, traditional blasting hole layouts have limitations such as clamping restrictions, inadequate rock fracture, and low utilization rates of explosive energy. The presence of an unfilled void can facilitate crack propagation and enhance fragmentation effectiveness.

Firstly, regarding the investigation of stress and damage distribution within the cavity cut area of the fragmented rock mass. The authors [1] posited that the tensile stress between the cavity and the rock mass was directly influenced by the void radius and conducted an analysis on stress concentration. The stress value at the void can be accurately calculated. Li et al. [2] have enhanced the calculation model for voids and established a correlation between the distribution position of hole wall stress and the influence of hole radius on stress. The parameter values in the void cut area were calculated by Zhang et al. [3] with a focus on various parameters, taking into account the stress concentration effect, the principle of dilatation space, and the free surface effect. The effectiveness of the blasting parameters was then verified through examples. The study conducted by Meng et al. [4] utilized numerical simulation to establish a constitutive model for rock mass damage under tensile and compressive loads in the cavity region. Their findings indicated that the presence of a cavity resulted in an increase in both tensile stress and stress concentration coefficient within the surrounding rock mass. The study conducted by Sun et al. [5] examined the arrangement of blasting holes in the excavation area and determined that alterations in hole layout parameters directly impacted the effectiveness of rock fragmentation within the excavation area. The entrance section of a high-speed railway tunnel blasting project was taken as an example by Gao et al. [6]. They optimized the parameters for wedge incision blasting using ANSYS/LS-DYNA software and, based on this optimization, effectively reduced vibrations while ensuring

CONTACT Yan Zhao 304965624@qq.com Hebei University of Architecture, Hebei 075000, People's Republic of China; School of Mechanics and Civil Engineering, China University of Mining and Technology (Beijing), Beijing 100083, People's Republic of China; Hebei Provincial Key Laboratory of Civil Engineering Diagnosis, Reconstruction and Disaster Resistance, Hebei 075000, People's Republic of China; Zhangjiakou BIM Engineering Technology Innovation Center, Zhangjiakou 075000, People's Republic of China

the desired blasting outcome. Zhao et al. [7] proposed a regression analysis approach that integrates signal preprocessing, dimension analysis, and particle swarm optimization to address the vibration attenuation law in tunnels. This methodology was successfully applied to a practical case study involving cross-tunnel blasting. Based on the Caomao Mountain tunnel project, The field monitoring and theoretical investigation of the blasting-induced vibration effect are conducted to assess the transverse tunnel, followed by an analysis of the dynamic response of the existing tunnel under instantaneous explosive loading [7]. The study conducted by Tian et al. [8] aimed to investigate the propagation characteristics of blasting vibration velocity in strata and mitigates the adverse effects of blasting vibrations on nearby structures through a series of tests carried out during the Dizong Tunnel project.

In summary, the existing models for calculating stress in hollow structures fail to accurately capture the evolution law. As a weak plane of discontinuity, empty voids alter the stress loading path of rock masses within explosion zones. The paper enhances the "thin cylinder model" based on the principles of elasticity and Saint-Venant, and establishes a theoretical analysis model for dynamically changing wall stress in circular voids. The optimal arrangement is proposed, demonstrating the dynamic mechanism of hole wall stress under longitudinal wave action, which significantly influences the loading path and failure effect of the excavated rock mass. The vibration effect of different types of void cut blasting on the surrounding environment is analyzed through rigorous calculation, comprehensive testing, and advanced simulation techniques.

2. Theoretical models for the damage caused by void cutting

When voids are present within the cut area, stress redistribution occurs near the hole wall, resulting in higher values of circumferential stress σ_θ. The stress wave reflection occurs when the explosion generates a stress wave that interacts with the free surface of the void hole. In this scenario, the compressive stress wave undergoes a transformation into a tensile stress wave, leading to the application of tensile forces on the rock mass surrounding the void hole wall. As a result, the damage mechanism observed in the hole wall is characterized by tensile failure [9, 10]. Due to the property of rock mass dilation, the volume of rock mass in the excavation area increases upon fragmentation, requiring additional space for compensation. Consequently, this phenomenon leads to rock regeneration and suboptimal utilization rate of blasting holes. The presence of vacant voids prompts the fractured rock to selectively propagate towards these voids, counteracting the swelling phenomenon and facilitating the expulsion of rocks.

The stress wave is considered as an equivalent load resulting from the infinite radius of the cylindrical wave at the void. The blasting process is divided into two distinct sections: Sections I and II. The diameter of the circular aperture is denoted by d, while the side length of the square aperture is represented by a. Therefore, a model can be constructed based on these specifications. The mechanical model assumes a homogeneous elastoplastic and isotropic rock mass to facilitate the study. The stress load is approximately equivalent to the uniform load, indicating a consistent distribution of particles with constant force.

2.1. The model employed is a thin-walled cylinder

The force analysis model for the rock mass of the borehole wall is established, as depicted in Figure 1, with a specific focus on investigating the void section of the borehole. When subjected to stress waves, the hole wall reaches a critical failure state, resulting in the formation of a slender annular structure [11, 12].

2.2. The model of a ring with thin walls

The stress analysis model for the rock mass of the borehole wall is established, as depicted in Figure 1, with specific research focal points identified. When subjected to stress waves, the hole wall undergoes failure in its critical state, resulting in the formation of a slender ring structure.

The uniform load q_2 is applied to the wall of the void, resulting in the generation of a reflected tensile wave at the same wall. In zone I, R_2 represents the radius of the void, while R_h denotes the thickness of its thin wall. Due to the significant difference in size between L_1 and R_h, there is a significant deviation in stress distribution between the rock mass surrounding the wall and that acting on the wall itself [13]. The elastic modulus of the rock mass outside the thin-walled ring is denoted as E', while the shear modulus is represented by G', and the lateral shrinkage coefficient is indicated as ν'. The thin-walled ring exhibits an elastic modulus of E, a shear modulus of G, and a lateral contraction coefficient ν. Among them, G' equals to E'/2(1+ν'), ν equals to μ_d /(1-μ_d), where μ_d represents the dynamic Poisson's ratio (0.8 times μ) and μ represents Poisson's ratio [3].

$$\begin{cases} \sigma_r = q_2 sin\theta \dfrac{[1+m'(1-2\nu_d)] \dfrac{(R2+Rh)^2}{r^2} - (1-m')]}{[1+m'(1-2\nu_d)] \dfrac{(R2+Rh)^2}{R2^2} - (1-m')]} \\ \sigma_\theta = -q_2 sin\theta \dfrac{[1+m'(1-2\nu_d)] \dfrac{(R2+Rh)^2}{r^2} + (1-m')]}{[1+m'(1-2\nu_d)] \dfrac{(R2+Rh)^2}{R2^2} - (1-m')]} \end{cases} \quad (1)$$

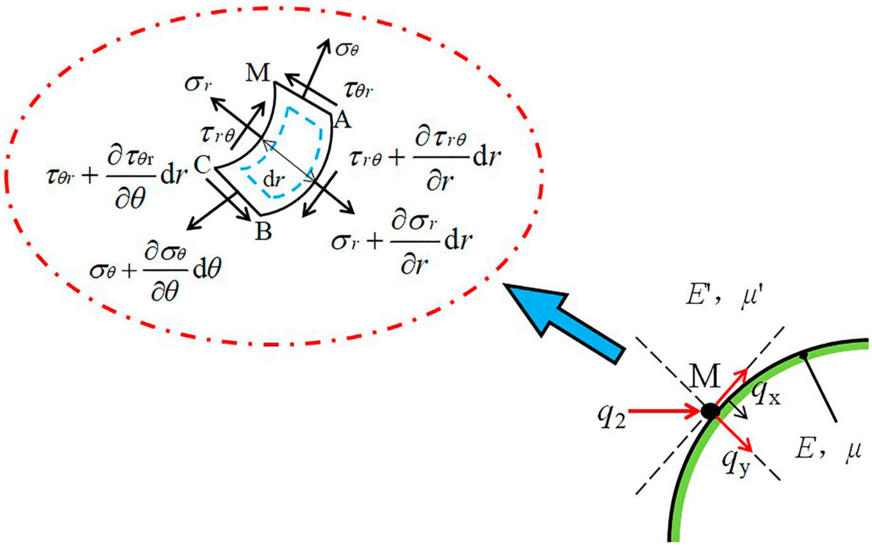

Figure 1. Illustrates the stress analysis diagram of a quarter circular void.

2.2.1. The principle analysis of the force exerted on a circular cavity wall

The force analysis of the microelement M is conducted, as shown in Figure 1. Here, σ_r represents the radial stress, σ_θ denotes the circumferential stress, and $\tau_{r\theta}$ and $\tau_{\theta r}$ represent the shear stresses. The element M has a radial thickness of dr and a circumferential angle of $d\theta$ [14, 15].

The expression of $[\sigma_\theta]$ is derived from the physical equation, where the strain of rock mass before the loss of stability is denoted as $[\epsilon_r]$ and $[\epsilon_\theta]$, and the stress is represented by $[\sigma_\theta]$:

$$[\sigma\theta] = \frac{1-\nu_d}{\nu_d}[\varepsilon\theta] + \frac{(2u-2){\nu_d}^2 + (2-3u)\nu_d + \nu_d - 1}{-2u{\nu_d}^2 + u\nu_d}[\varepsilon r] \tag{2}$$

Among them, $[\epsilon_\theta] > \epsilon_\theta > 0$, $[\epsilon_r] > \epsilon_r > 0$, $[\epsilon_r]$ and $[\epsilon_\theta]$ coefficient increases with the decrease of the ν, the effect of radial stress enhanced hoop stress. The circumferential stress σ_θ induces extrusion in the surrounding rock of the borehole wall, while the presence of a circular void within the wall prevents radial shear stress during circumferential loading. Simultaneously, the circular void wall can effectively protect against destruction of the rock mass.

2.3. Model of a square void in the wall surface

The enhanced model, as shown in Figure 2, incorporates a "square aperture" to accurately contrast with the circular aperture model while maintaining an equivalent cross-sectional area of the aperture. Let's denote the side length of the square aperture as "a" (where $a = 1.772R_2$).

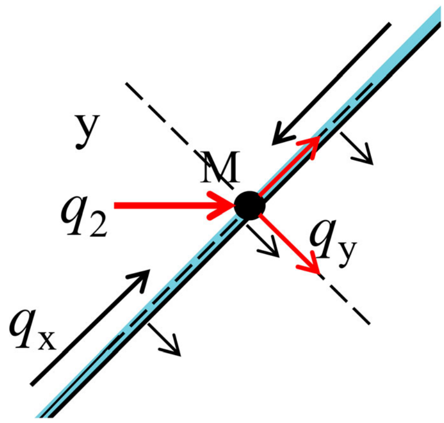

Figure 2. The force analysis of a quarter section of an empty square aperture.

The complex function is introduced to address the stress issue associated with the square opening [16–19]. The square aperture wall is subjected to an equivalent uniform load, denoted as q_2. Point M is selected for investigation, where the load q_2 can be decomposed into qx and q_y components with $q_x = q_y = 0.886\, q_2$. At the boundary of the square aperture, there exist $r = 1$, $\zeta = e^{i\theta}$, $\sigma_r = \tau_{r\theta} = 0$ conditions. The expression for σ_θ stress can be calculated as follows [20]:

$$\sigma\theta = q_2(1+\nu_d)\frac{3n1n2 - 14n1\alpha 2\cos 4\theta - 14\alpha 2(1+7\alpha 2)\sin^2 4\theta}{n1^2 + (1+7\alpha 2)\sin^2 4\theta} \tag{3}$$

Among them: $n_1 = 3\alpha_1 + (7\alpha_2\text{-}1)$, $n_2 = 3s_1/(A \times B)$, $\alpha_1 = -0.167$, $\alpha_2 = 0.018$. By calculating formula (1) and formula (3), the circumferential stress at the corner of the square void is 11.76 q_2, the stress at the center of the hole edge is -2.79 q_2, the radial stress at 0° and 45° of the circular void is q_2 and 1.414 q_2, and the circumferential stress is -1.176 q_2 and -1.663 q_2.

3. The simulation and analysis of numerals

3.1. The process of constructing a model

When developing the theoretical framework, despite being based on specific assumptions, the practical procedure of drilling and blasting is exceedingly complex. To enhance our understanding of this process, I utilized the sophisticated numerical simulation tool ANSYS/LS-DYNA and creatively incorporated a tensile-compressive damage mechanism into the foundational material model. To address the challenges arising from large deformation and highly nonlinear dynamic processes, we have employed the multi-material Arbitrary Lagrangian-Eulerian (ALE) fluid-solid coupling algorithm, which accurately models interactions among complex physical fields. Moreover, in order to ensure the authenticity of our simulation results, non-reflective boundary conditions have been implemented on the model boundaries to mitigate their influence on internal dynamic processes [21].

The 2# rock emulsion explosive model was established using LS-DYNA, and the corresponding parameters are presented in Table 2. By employing a coupled charge approach, the detonation pressure and relative volume of the detonation product were described by utilizing the JWL equation:

$$P = A\left(1 - \frac{\omega}{VR_1}\right)e^{-R_1 V} + B\left(1 - \frac{\omega}{VR_2}\right)e^{-R_2 V} + \frac{\omega E_0}{V} \quad (4)$$

The initial detonation pressure P, expressed in mega Pascal's (MPa), is a crucial parameter that characterizes the initial strength of explosive pressure during detonation. The volume V of the detonation products, measured in liters (L), reflects the spatial expansion of the explosion products. The initial specific internal energy E_0 is a significant indicator of the internal energy density of the explosive, directly related to the power and effect of the explosion. A, B, R_1, R_2, and ω are constants closely associated with the blasting process and utilized in the JWL (Jones-Wilkins-Lee) state equation to precisely describe the pressure-volume relationship of detonation products, thereby influencing characteristics of explosion wave and energy release.

Table 1. Parameters for blasting hole.

Breeching /(mm)	Void/(mm)	s_1/(mm)	s_2/(mm)	s_3/(mm)	s_4/(mm)
32	200/180	600	850	850	1,500

The cut-hole blasting model configuration is illustrated in Figure 3, while the relevant parameters are presented in Table 1.

The rock model parameters are presented in Table 3 [22].

3.2. The verification of model reliability

The experiment utilized a Plexiglas plate (PMMA) as the substitute material, which displayed favorable brittle failure characteristics when exposed to an explosion. The glass plate was designed with dimensions of 50 mm × 50 mm × 4 mm, and the corresponding data are presented in Table 4. Figure 4 illustrates the observed trend of damage after conducting 5 SPBH impact tests.

The consistent trends of change are observed through the comparison of experiments, theoretical calculations, and simulations. Although there are variations in numerical values among the parameters of the test materials, the basic values set by the numerical model and the recommended theoretical model, the results consistently demonstrate a similar pattern of damage. Therefore, both the theoretical model and simulation can be considered reliable.

3.3. Trend in the distribution of stress

The equivalent stress is a parameter that objectively indicates the failure condition of rock mass materials and adheres to the invariance principle of the fourth strength theory (shape-specific energy theory). Figure 5 illustrates the nephogram of equivalent stress and crack

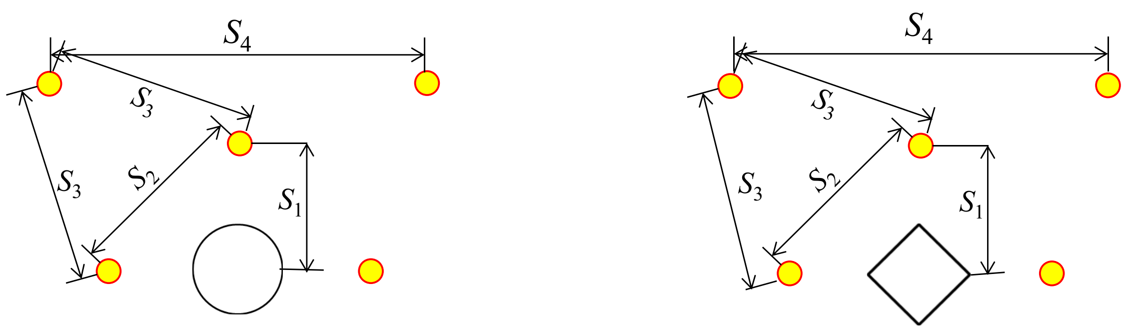

Figure 3. The layout of the semi-sectioned area. Note: Length of side = 180 mm, Radius = 200 mm.

Table 2. Exploded material parameters.

Density /(g·cm^{-3})	Detonation velocity /(m·s^{-1})	Detonation pressure /GPa	*A* /GPa	*B* /GPa	R_1	R_2	ω	E_0 /GPa
1.02	4700	27.5	286	0.83	5.12	1.98	0.53	3.8

Table 3. Parameters of the rock model.

Density /(g·cm^{-3})	Poisson's ratio	Compressive strength /MPa	Tensile strength /MPa	Shear strength /MPa	Modulus of elasticity /GPa
2.7	0.32	95.9	6.5	13.6	25.6

propagation in porous rock mass under P-wave action [5,23–25,35].

The consistent contour distribution observed in both cloud charts suggests that the rock mass beyond the fracture zone is subjected to stress and exhibits tensile fractures. By comparing the results of hollow damage, it becomes evident that there is a higher occurrence of interconnected hollows surrounding the square-shaped cavity within Zone I. The presence of circular hollow walls hinders the formation of a ring-like structure around each cavity, thereby reducing the tensile effects caused by reflected waves. Subsequent stress wave segments facilitate interconnection among fractures occurring outside cavities, resulting in lateral fissures between adjacent cavities due to variations in wall resistances.

4. Repercussions of vibration in regions beyond the excavation zone

The primary concern of tunnel blasting lies in its detrimental impact on existing tunnels, chambers, and surface structures in close proximity to the explosion site. Accurately ascertaining both the maximum direction and intensity of vibrations is crucial for safety measures. Therefore, comprehensive vibration monitoring is conducted for circular and square hole cut layouts to assess the attenuation of vibration velocity [26–29].

4.1. The arrangement of measuring points

The rock mass surrounding the excavated area is equipped with monitoring points positioned at 45° and 90° angles, as depicted by the circular region in the diagram. In each direction, five strategically placed

Table 4. The simulated value of peak velocity for blasting-induced vibrations.

	45° Direction				90° Direction			
	First stage	Second stage	First stage	Second stage	First stage	Second stage	First stage	Second stage
0	0	0	0	0	0	0	0	0
0.2	1.75	1.512	2.133	2.497	2.399	1.137	2.371	1.398
0.4	1.509	1.119	1.687	1.312	1.479	1.156	1.625	1.149
0.6	1.248	0.715	1.311	1.099	1.194	1.584	1.043	1.747
0.8	1.127	0.594	1.188	0.784	0.761	1.351	0.907	1.542
1.0	0.923	0.499	1.044	0.603	0.759	1.287	0.772	1.513
1.2	0.021	0.0124	0.354	0.341	0.076	0.036	0.068	0.106
1.4	0.0135	0.00923	0.262	0.257	0.048	0.021	0.053	0.089
1.6	0.007	0.00512	0.156	0.164	0.011	0.005	0.01	0.043
1.8	0.001	0.00085	0.071	0.0657	0.005	0.002	0.006	0.011
2.0	0.0005	0.00023	0.025	0.011	0.001	0.0009	0.0013	0.009

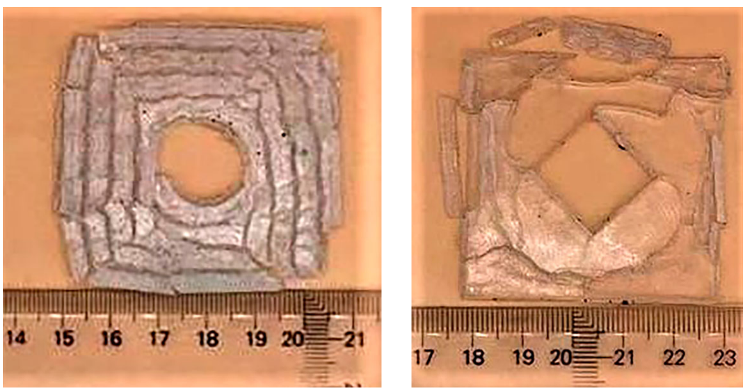

(a) (b)

Figure 4. Results of damage distribution in SPBH longitudinal wave impact test. (a) Experimental findings of a round cavity specimen subjected to a longitudinal wave; (b) Experimental findings of a square cavity specimen subjected to a longitudinal wave.

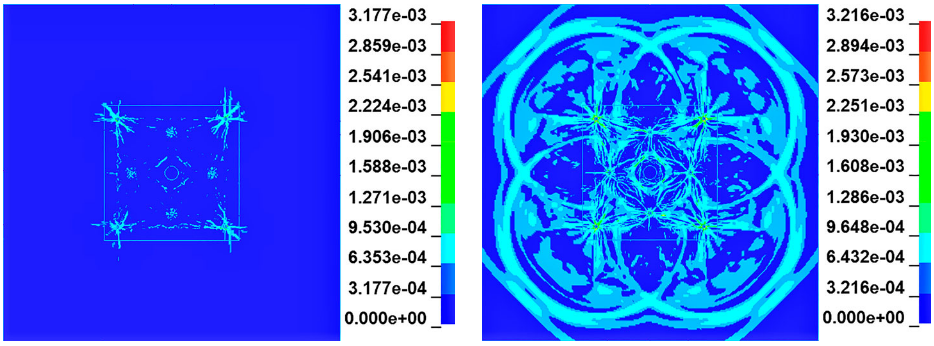

(1) Von-Mises stress analysis of a circular void

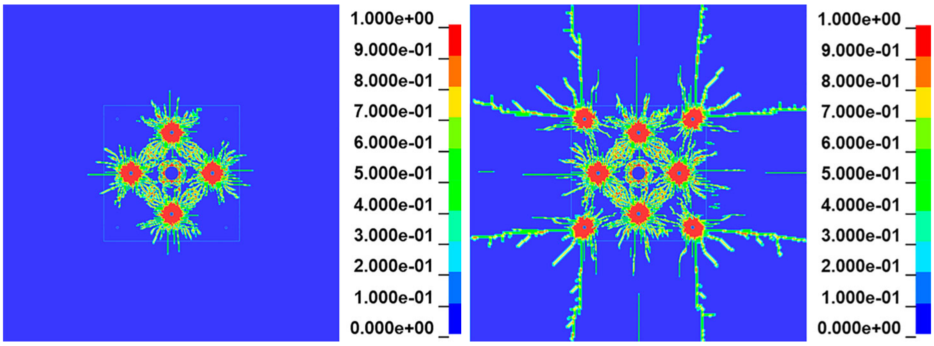

(2) Image of a circular void model depicting the destructive effects of explosive blasting

(a)

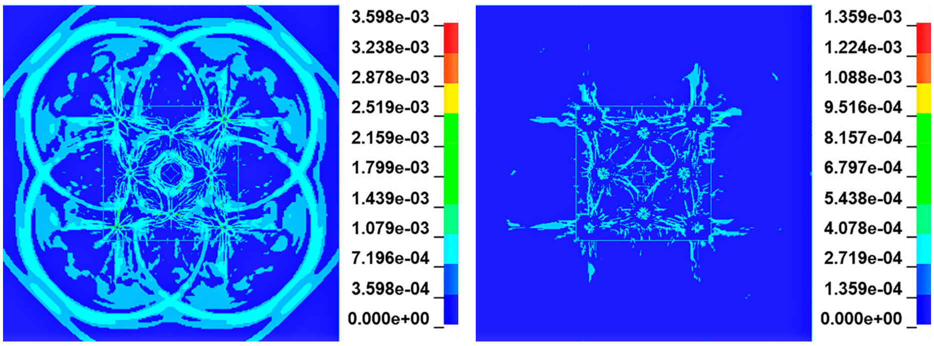

(1) Von-Mises stress analysis of a square void

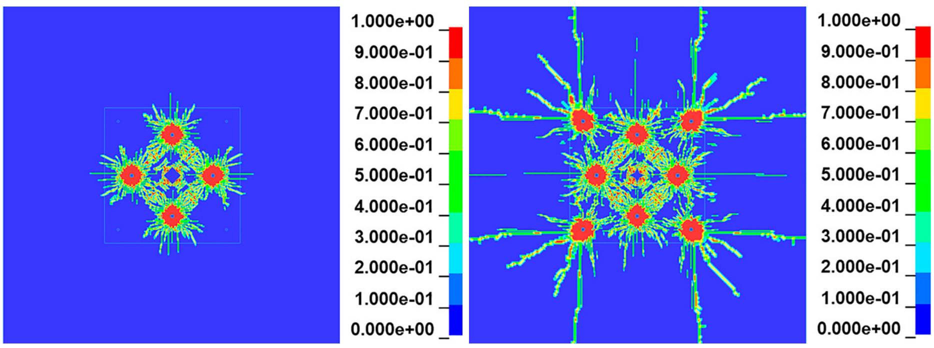

(2) Image of a square void model depicting the destructive effects of explosive blasting

(b)

Figure 5. Stress equivalence and the evolution of damage. (a) Recesses characterized by circular voids; (b) Recesses characterized by square voids. (1) Von-Mises stress analysis of a circular void; (2) Image of a circular void model depicting the destructive effects of explosive blasting.

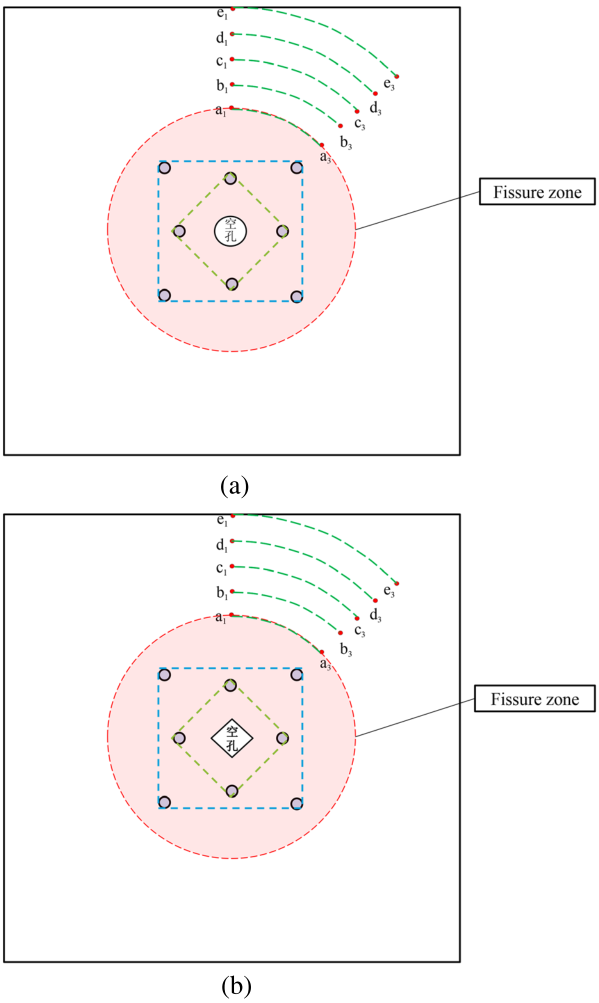

Figure 6. The arrangement of measuring points in the rock mass outside the excavation area. (a) The arrangement of measuring points in a circular void; (b) The arrangement of measuring points in a square void.

points monitor vibrations occurring around the excavation site [30–32]. Additionally, a measuring point is installed in the central area to monitor the vibration impact caused by cutting hole explosion, as illustrated in Figure 6.

4.2. Analysis on the impact of vibration on peripheral rock mass

4.2.1. Reverberation is observed in the central region of the perforated aperture

As shown in Figure 7.

If the energy generated by the explosion is directed towards crushing the rock mass instead of dissipating outward, it optimizes the cutting effect and reduces vibration in the surrounding rock mass. Figure 7 illustrates the peak attenuation curve of vibrations in the central region of the excavation area. The attenuation trend for both types of boreholes is similar. Vibration levels at the center of a circular void measure 382 cm/s, while those at the center of a square void measure 263 cm/s. Subsequently, vibrations at a circular hole's center fluctuate between 85 cm/s, whereas those at a square void fluctuate between 49 cm/s. This discrepancy arises due to changes in energy distribution caused by circular voids, where explosive energy escapes through these openings; conversely, square voids enable a more efficient utilization of explosion energy for rock fragmentation (Figure 8).

4.2.2. Cumulative vibration velocity of the rock mass beyond the excavation zone

(1) The vibration velocity in the direction of 45 degrees

As shown in Figure 8, the maximum vibration velocity in the 45° direction is 17.6 cm/s at $t = 310\ \mu s$ for the circular void cut hole, and 25.0 cm/s at $t = 280\ \mu s$ for the square void cut hole. However, according to the attenuation law shown in the figure, it can be observed that the peak vibration velocity of the circular void cut model is slightly greater than that of the square void cut model. While the vibration generated by the explosion of the square void cut model diminishes and approaches zero after $t = 1$ ms, the circular void cut model consistently maintains a stable value equivalent to that of a non-cut rock throughout its entire attenuation process. Consequently, it can be inferred that having a square void has minimal impact on rock vibrations in a 45° direction.

(2) The vibration velocity in the direction of 90 degrees

The maximum value of the 90° combined vibration velocity is 23.6 cm/s at $t = 100$ µs in the circular void cut hole, and it is 23.5 cm/s at $t = 99.9$ µs in the square void cut hole, as depicted in Figure 9. The vibration intensity remains consistent between the circular and square void cut hole models.

By analyzing the attenuation law of combined vibration velocity in both the 45° and 90° directions, it is observed that vibrations are more pronounced in the vertical direction of the tunnel resulting from both types of cut hole blasting. Furthermore, when considering blasts at a 45° angle, square void cut models have a greater impact on vibrations compared to circular voids. Nevertheless, due to inconsistent distances between measurement point's a_1 and a_3 relative to each blasting hole, there might be noticeable errors in peak vibration velocity. However, since both the first point in the vertical direction and the second point in the 45° directions are equidistant from their respective blasting holes, their vibration velocities remain identical [18,33,34]. The vibration velocity diagram reveals that the square void primarily concentrates its vibration energy on crushing the rock mass in the cut area during the initial stage of blasting, while subsequently attenuating the vibrations transmitted to the outer rock mass.

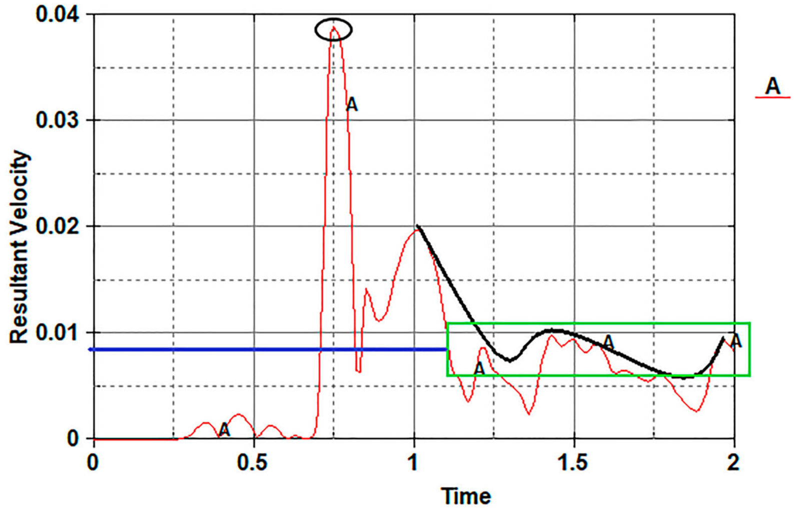

(a)

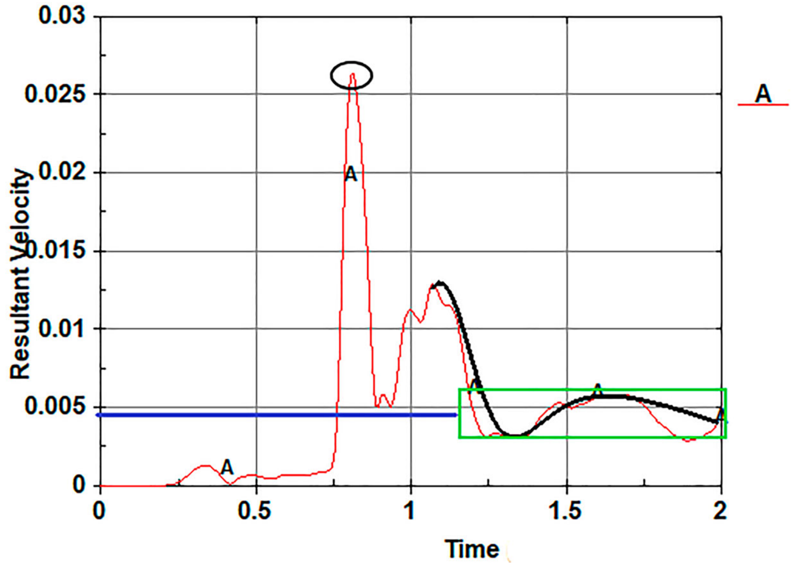

(b)

Figure 7. Vibration attenuation profile within the central region of the excised area. (a) Combined vibration velocity of the circular void; (b) Combined vibration velocity of the square void.

4.2.3. Theoretical calculation

The vibration attenuation data were computed by optimizing the model, as presented in Tables 4 and 5.

Due to inherent difficulties in accurately calculating the driving force of explosive gas, theoretical calculations slightly underestimate its value compared to numerical simulations. This research further confirms the benefits of using square void cut blasting techniques and demonstrates that when combined with SPBH longitudinal wave testing, it is observed that most of the energy within a square void contributes significantly to fracturing rocks in cutting areas. Moreover, in a round hole model, an initial damage ring caused by stress waves serves as an impedance barrier against subsequent stress waves and exhibits a "continuous oscillation" characteristic when responding to external vibrations.

5. Conclusions

By conducting analysis, calculations, and making improvements on the blasting mode of the cut zone, we enhance its crushing effect. Furthermore, we establish a monitoring scheme for blasting vibrations. Compared to the circular void model, the square void model demonstrates quicker attenuation of vibrations in the surrounding rock mass. Additionally, while ensuring effective cutting operations are carried out successfully during blasting processes themselves reduce external vibration response.

(1) During the stress process of a rock mass in a hollow wall, its impedance characteristics hinder the initiation of failure. As dynamic stress gradually increases, a distinct "layered annular failure" mode

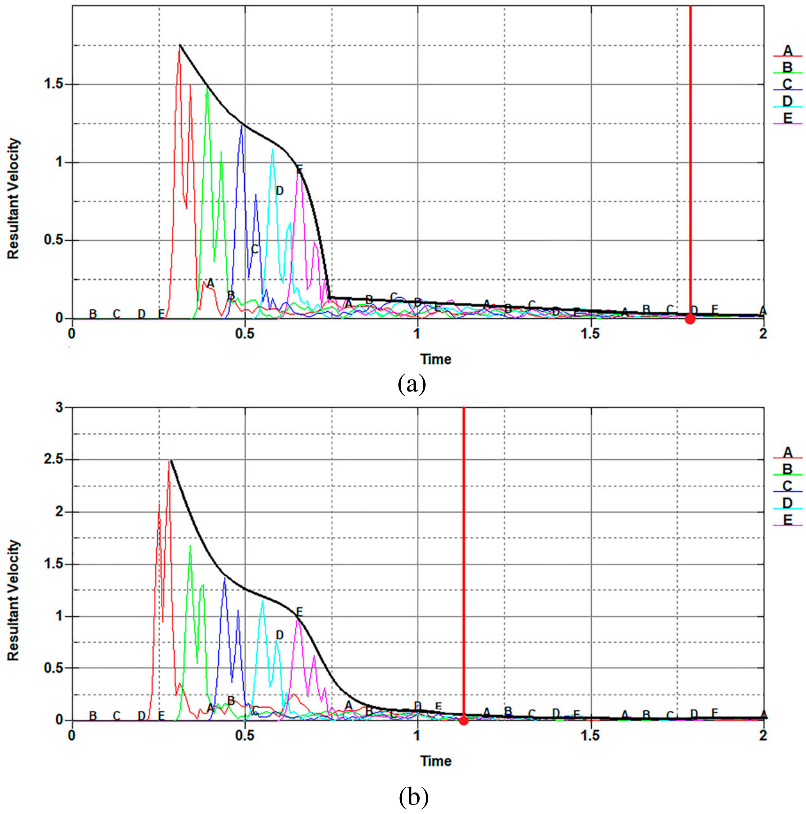

Figure 8. Attenuation curve of vibration velocity in the 45° open void mode. (a) The curve of blasting and vibration velocity for a circular cavity mode; (b) The curve of blasting and vibration velocity for a square cavity mode.

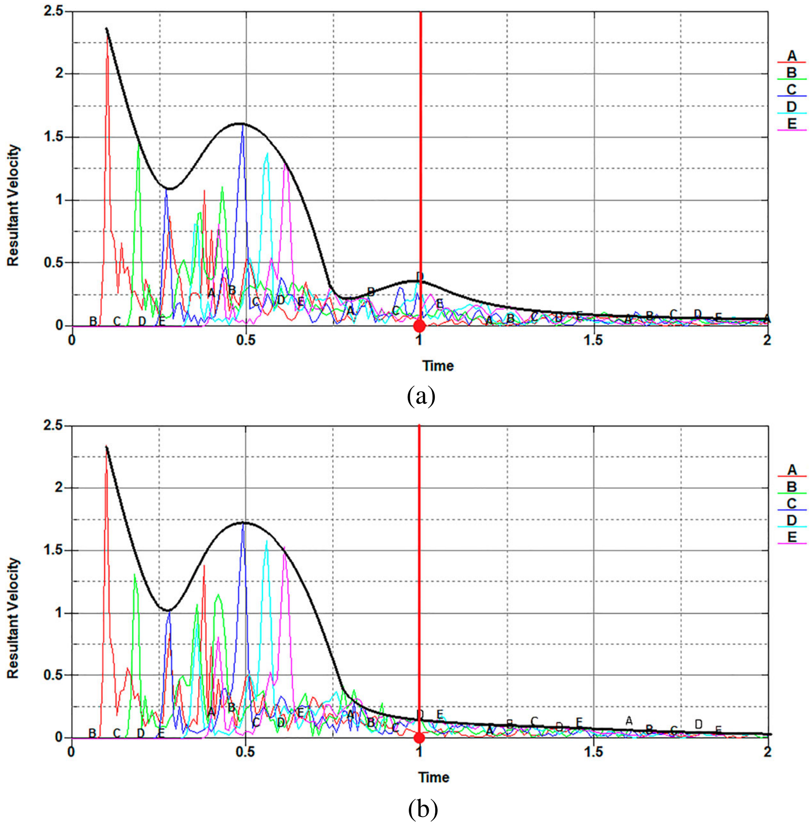

Figure 9. Attenuation curve of vibration velocity in a 90° open void mode. (a) Velocity curve of blasting-induced vibrations in a circular cavity model; (b) Velocity curve of blasting-induced vibrations in a square cavity model.

Table 5. The calculation of peak velocity for blasting vibration.

	45° Direction				90° Direction			
	First stage	Second stage	First stage	Second stage	First stage	Second stage	First stage	Second stage
0	0	0	0	0	0	0	0	0
0.2	1.69	1.509	2.115	2.476	2.324	1.121	2.342	1.387
0.4	1.489	1.107	1.679	1.253	1.456	1.146	1.587	1.142
0.6	1.245	0.736	1.31	0.996	1.103	1.106	0.989	1.058
0.8	1.118	0.556	1.182	0.716	0.684	1.064	0.851	0.976
1.0	0.903	0.451	0.953	0.553	0.726	0.975	0.702	0.831
1.2	0.023	0.0125	0.341	0.32	0.071	0.034	0.059	0.102
1.4	0.0136	0.0093	0.264	0.251	0.049	0.018	0.043	0.845
1.6	0.006	0.0051	0.15	0.158	0.01	0.004	0.009	0.389
1.8	0.001	0.00083	0.069	0.052	0.004	0.0021	0.005	0.1
2.0	0.00049	0.00021	0.0023	0.01	0.0009	0.0007	0.001	0.007

is observed in the rock mass surrounding the circular cavity wall, while a multi-layer tensile damage state occurs in the rock mass around the square cavity wall with prolonged damaging effects. The circumferential impedance mechanism of a circular void primarily dissipates energy from explosion stress waves through compression and crushing of the hole wall, thereby limiting further propagation of stress waves within the rock. In contrast, explosion stress waves generated by cut holes tend to induce tensile failures in the rock mass. Additionally, residual vibrations are more pronounced in circular cavity models compared to square cavity models.

(2) In the central region of the excavation zone, the shape effect results in a greater concentration of energy into the central area for circular hole excavations, while square hole excavations direct more energy towards rock mass fracturing. Consequently, the outgoing vibration energy is comparatively lower in square hole models than in circular hole cut models. During the initial stage of blasting, vibrations generated by square holes are slightly larger than those from round holes at a 45° angle outside the excavation zone. However, after 1.1 ms, vibrations produced by square hole models decrease at a faster rate. In the 90° direction, attenuation in vibration velocity is more stable and lower for square voids compared to circular voids after 1 ms.

Based on the current damage model, this study only presents the instantaneous characteristics of the blasting effect. Currently, there has been no detailed investigation into the impact of shear effects generated by axial micro-element charges on cutting efficiency. It is anticipated that future research will incorporate a three-dimensional damage model for prediction purposes. Additionally, it should be noted that the proposed theoretical model assumes rock mass as an elastic body and does not account for the influence of ground deformation in voids on stress loading paths and damage in a plastic state.

Acknowledgements

The research presented in this work is financially supported by the National Natural Science Foundation of China (No.: 51878242), the Doctoral Degree Start-up Fund project of Hebei University of Civil Engineering and Architecture (B-202304), the cooperation project between the Scientific Research Industry Division of Hebei University of Civil Engineering and Shijiazhuang Construction Engineering Group Co., LTD. (No.: 241790797A), and the Hebei University Research Project (BJK2024118).

Disclosure statement

No potential conflict of interest was reported by the author(s).

Author contributions

Huifeng Qin: Writing – original draft (equal). Yan Zhao: Writing – review & editing (equal). Hailong Wang: Data curation (equal). Lijie Ge: Writing – review & editing (equal).

Data availability statement

The data that support the findings of this study are available from the corresponding author upon reasonable request.

References

[1] Lin D N, Chen S R. Theory and practice analysis of cavity formation model of straight hole cutting with void. Rock Soil Mech, 2005;03:479–483. doi:10.16285/smj.r.2005.03.029.

[2] Li QY, Wu ZY, Huang WL. Calculation model of cylinder cut void effect improvement and analysis. J Mining Safety Eng. 2018;35(5):925–930. doi:10.13545/j.carolcarrollnkijmse.2018.05.007. (in Chinese)

[3] Zhang ZR, et al. Study on hollow effect and blasting parameters of straight holes cut with hollow holes. J China Coal Soc. 2020;45(S2):791–800. doi:10.13225/j.cnki.jccs.2019.1591

[4] Meng NK, et al. Damage evolution mechanisms of rock induced by blasting with the aid of empty-hole effect. Energies. 2020;5(8):1824–1839. doi:10.3390/en13030756

[5] Sun HS, et al. Analytical investigation of tunnel deformation caused by circular foundation pit excavation.

Comput Geotech. 2019;106:193–198. doi:10.1016/j.compgeo.2018.11.001
[6] Gao WL, Liu Z, Wang Y, et al. Study on optimization of delay method of wedge cut blasting in tunnel. Shock Vib. 2021;2021:1–15.
[7] Zhao Y, Shan RL, Wang HL, et al. Vibration response and evaluation system of cross–tunnel blasting. Bull Eng Geol Environ 81. 2022:417. doi:10.1007/s10064-022-02911-9.
[8] Tian XX, Song ZP, Wang JB. Study on the propagation law of tunnel blasting vibration in stratum and blasting vibration reduction technology. Soil Dyn Earthq Eng. 2019;126:105813. doi:10.1016/j.soildyn.2019.105813.
[9] Chen BB, et al. Design and application of blasting parameters for presplitting hard roof with the aid of void effect. Shock Vib. 2018:16. doi:10.1155/2018/8749415.
[10] Liu CW, et al. Directional fracturing by slotting-blasting-caused stress wave form changes. J Int J Impact Eng. 2019;02:141–151. doi:10.1016/j.ijimpeng.2019.02.002
[11] Xu SD, et al. Optimization of blasting parameters for an underground mine through prediction of blasting vibration. J Vib Control. 2019a;25(9):1585–1595. doi:10.1177/1077546319829938
[12] Xu XD, et al. A new calculation model of blasting damage degree-based on fractal and tie rod damage theory. Eng Fract Mech. 2019;220:106619. doi:10.1016/j.engfracmech.2019.106619.
[13] Li XP, et al. Numerical simulation research of smooth wall blasting using the timing sequence control method under different primary blast hole shapes. Shock Vib. 2019;16. doi:10.1155/2019/2425904.
[14] Pi YL, et al. Nonlinear analysis and buckling of elastically supported circular shallow arches. Int J Solids Struct. 2007;44(7):2401–2425. doi:10.1016/j.ijsolstr.2006.07.011
[15] Huang CX. Comparison of Mechanical properties of circular and parabolic arch structures. Building Struct. 2017;47:443–446. in Chinese doi:10.19701/j.jzjg.2017.s1.101.
[16] Milan B. On the stress concentration around a hole in an infinite plate subject to a uniform load at infinity. Int J Mech Sci. 2011;53(4):254–261. doi:10.1016/j.ijmecsci.2011.01.006
[17] Verruijt A. Deformations of an elastic half plane with a circular cavity. Int J Solids Struct. 2019;35(21):2795–2804. doi:10.1016/S0020-7683(97)00194-7.
[18] Zhang ZZ, et al. Analytical solution for a deep tunnel with arbitrary cross section in a transversely isotropic rock mass. Int J Rock Mech Min Sci. 2011;48(4):1359–1363. doi:10.1016/j.ijrmms.2011.10.001
[19] Mihir MD, et al. Stress concentration at the corners of polygonal holes in finite plate. Aerosp Sci Technol. 2016;58:197–206. doi:10.1016/j.ast.2016.08.014.
[20] Zan CY, et al. Distribution law and case study of surrounding rock stress in rectangular roadway. Coal Sci Technol. 2022;50(S1):112–118. in Chinese.
[21] Ji DW, et al. Stress rupture life prediction method for notched specimens based on minimum average von-mises equivalent stress. Metals (Basel). 2021a;11(7):2–8. doi:10.3390/met12010068
[22] Bartlomiej K, et al. Emulsion explosives: a tutorial review and highlight of recent progress. Materials (Basel). 2022;05:3–8. doi:10.3390/ma15144952
[23] Yang Z, et al. Factors affecting casing equivalent stress in multi–cluster fracturing of horizontal shale gas wells: finite element study on Weirong block, southern Sichuan Basin, China. J Petroleum Explorat Product Technol. 2023;13:1669–1689. doi:10.1007/s13202-023-01629-y
[24] Ji L, et al. Numerical studies on the cumulative damage effects and safety criterion of a large cross-section tunnel induced by single and multiple full-scale blasting. Rock Mech Rock Eng. 2021b;09:3–5. doi:10.1007/s00603-021-02630-9
[25] Hossein RR, et al. Forty-year review of the Hoek-Brown failure criterion for jointed rock masses. Rock Mech Rock Eng. 2021;10:2–5. doi:10.1007/s00603-021-02661-2
[26] Zhao Y, Shan RL, Wang HL, et al. Regression analysis of the blasting vibration effect in cross tunnels. Arab J Geosci. 2021;14(18). doi:10.1007/s12517-021-08257-y
[27] Xu YQ, Liu K, He BL, et al. Risk pre-assessment method for regional drilling engineering based on deep learning and multi-source data. Petroleum Sci. 2023;20(6):3654–3672. doi:10.1016/j.petsci.2023.06.005
[28] Zhu FH, Liu ZG, Huang AC. The shaped blasting experimental study on damage and crack evolution of high stress coal seam. J Loss Prev Process Ind. 2023;83. doi:10.1016/j.jlp.2023.105030.
[29] Zhu FH, Liu ZG, Huang AC. Study on the coupling mechanism of shaped blasting and void to crack coal body. Process Saf Environ Prot. 2023;175:644–653. doi:10.1016/j.psep.2023.05.078
[30] Huo XF, et al. Attenuation characteristics of blasting stress under decoupled cylindrical charge. Rock Mech Rock Eng. 2023;50:4185–4209. doi:10.1007/s00603-017-1274-3
[31] Song ZF, et al. Identifying delay time of detonator for a millisecond blasting. Adv Civil Eng. 2021:1–8. doi:10.1155/2021/5592696.
[32] Song YQ, et al. Study on the decoupled charge effect in deep-holes cumulative blasting of coal seam. Adv Civil Eng. 2019:8486198. doi:10.1155/2019/8486198.
[33] Gao GY, et al. Analytical elasto-plastic solution for stress and plastic zone of surrounding rock in cold region tunnels. Gold Regions Technol. 2012;72:50–57. doi:10.1016/j.coldregions.2011.11.007
[34] Li XP, et al. Numerical study on crack propagation of rock mass using the time sequence controlled and notched blasting method. Eur J Environ Civil Eng. 2021;26(13):6714–6732. doi:10.1080/19648189.2021.1956597
[35] Yang LY, et al. Fracture mechanism due to blast-imposed loading under high static stress conditions. Int J Rock Mech Min Sci. 2018;07:150–158. doi:10.1016/j.ijrmms.2018.04.039
[36] Yang RS, et al. Crack propagation behavior in slit charge blasting under high static stress conditions. Int J Rock Mech Min Sci. 2019;119:117–123. doi:10.1016/j.ijrmms.2019.05.002